ELSEVIER

Journal of Nuclear Materials 283–287 (2000) 832–837

journal of nuclear materials

www.elsevier.nl/locate/jnucmat

Fatigue behavior and development of microcracks in F82H after helium implantation at 200°C

J. Bertsch [a], S. Meyer [b], A. Möslang [c,*]

[a] *Heraeus GmbH, P.O. Box 1553, 63405 Hanau, Germany*
[b] *University Karlsruhe, IZSM, P.O. Box 3640, 76021 Karlsruhe, Germany*
[c] *Forschungszentrum Karlsruhe, Institute of Materials Research, P.O. Box 3640, 76021 Karlsruhe, Germany*

Abstract

The ferritic/martensitic steel F82H-mod has been push–pull fatigue tested at 200°C before and after homogeneous implantation of 400 appm helium at about 0.5 dpa and 250°C to assess the growth characteristics of short fatigue cracks and their impact on lifetime. Crack initiation and propagation on carefully polished specimen surfaces were monitored by a high resolution optical microscope during fatigue testing. Subsequent metallographic and microstructural investigations revealed crack initiation mainly along martensitic laths and transgranular crack propagation, partly affected by the orientation of martensitic bands in adjacent grains. A statistical analysis of the crack formation and propagation processes was performed. Irradiation has led to pronounced fatigue life reduction by a factor of ~5 at higher strain ranges and to a moderate fatigue life enhancement at low strain ranges. This behavior can be understood by different types of microstructural barriers and their effect on crack formation and growth.

1. Introduction

During the past years ferritic/martensitic steels of type 7–10% Cr–WVTa have been developed that satisfy not only the criteria of reduced long-term activation but also show significantly improved impact and fracture toughness properties [1,2]. The loading of structural materials in fusion reactors is, besides the plasma surface interactions, a combined effect of high heat fluxes and neutron irradiation. Next step fusion devices can be characterized by plasma burn and off-burn periods generating thermal cycling. Depending on the pulse lengths, the operating conditions, and the thermal conductivity, these oscillating temperature gradients will cause elastic and elastic–plastic cyclic deformation giving rise to (creep-) fatigue in structural first wall and blanket components.

In the present fusion technology programs of reduced activation ferritic/martensitic steels, efforts concentrate on critical issues such as irradiation hardening at temperatures below about 320°C, embrittlement phenomena due to helium and hydrogen, and understanding of all relevant micromechanisms that control fracture resistance. A specific feature of fusion neutrons is helium production rates of about 100 appm/yr that cannot be matched adequately by conventional irradiation programs based on fission reactors or charged particle accelerators. Lifetime predictions for reactor components require the generation of a suitable database with mechanism-oriented descriptions of the fatigue damage. For these purposes, a cyclotron based irradiation program with relevant helium accumulation was performed on suitable fatigue specimens with carefully polished surfaces. The application of a high resolution long-range optical microscope with subsequent scanning and transmission electron microscopy analyses allows a direct correlation between crack morphology, microstructural details and fatigue data. Based on these methods, results for postirradiated and unirradiated push–pull fatigue

* Corresponding author. Tel.: +49-7247 82 4029; fax: +49-7247 82 4567.
E-mail address: anton.moeslang@imf.fzk.de (A. Möslang).

0022-3115/00/$ - see front matter
PII: S0022-3115(00)00313-5

samples made of F82H-mod steel are presented and discussed.

2. Experimental

The material used for these investigations was part of the international reference heat F82H-mod that is characterized presently within the frame of an IEA coordinated international program. The chemical composition is listed e.g., in [1]. The tested hollow specimens had a wall thickness of 0.40 mm, a gauge length of 10 mm, and their square cross-section was optimized by advanced elastic–plastic finite element calculations in order to meet the requirements for well defined uni-axial fatigue testing. Within a broad load range and temperature window the fatigue properties of this hollow specimen are in good agreement with results derived from conventional specimen geometries [3]. The heat treatment following fabrication consisted of 1040°C/0.5 h + 750°C/1 h resulting in a fully tempered martensite with carbides mainly of type $M_{23}C_6$ which lie along former austenite grain boundaries and lath boundaries.

Prior to fatigue testing several fatigue specimens were irradiated at a blanket relevant temperature of 250°C with a degraded 104 MeV α-particle beam to get a homogeneous concentration of 400 appm helium within the gauge volume. An additional induction coil heating system prevented temperature gradients in the gauge volume and maintained the temperature during experiments on unirradiated specimens. The irradiation conditions are given in Table 1. Using an axial high temperature extensometer clamped in the central part (5 mm) of the gauge length, continuous strain controlled push–pull cycling has been applied at 200°C with a cycle ratio of $R = -1$, a total strain range of $\Delta\varepsilon_t = 0.4$–$0.9\%$, and a strain rate of $\dot{\varepsilon} = 8 \times 10^{-4}\ s^{-1}$ corresponding to loading frequencies of about 0.1 Hz and less.

Table 1
Parameters of the α-particle implantations

Irradiation temperature	250°C
Environment specimen outside	Vacuum ($<10^{-3}$ Pa)
Environment specimen inside	Purified He-gas (2×10^5 Pa)
α-particle energy	0–104 MeV
Damage production rate	$(0.6–2) \times 10^{-6}$ dpa/s
Helium production rate	$(6–12) \times 10^{-4}$ appm He/s
Helium concentration	400 appm
Displacement damage dose	(0.40–0.67) dpa

During every fatigue test, data acquisition included (i) recording of several hundred stress–strain hysteresis loops, and (ii) optical microscope sampling of several hundred scans with a surface area of $7.0 \times 10.0\ mm^2$ by triggering the camera automatically at maximum strain at a predefined cycle N. The analysis of the surface

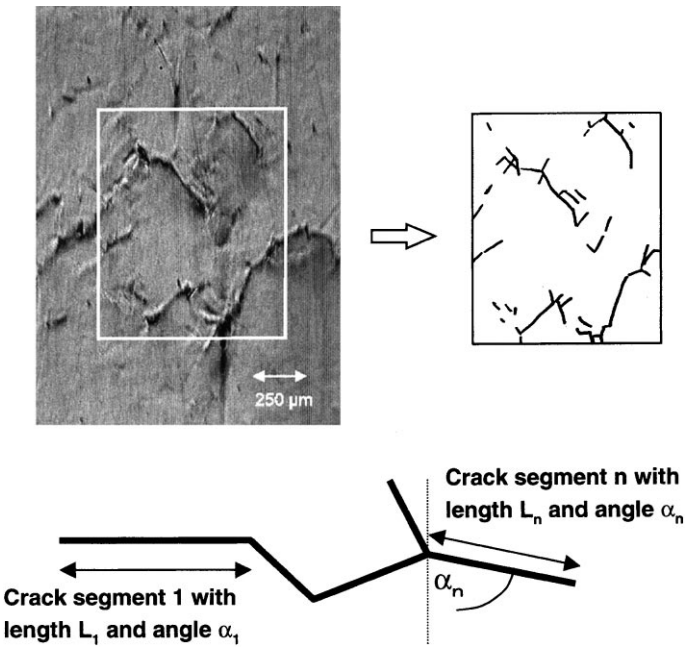

Fig. 1. Analysis and characterization of surface cracks at cycle N during strain controlled fatigue tests using a high resolution long range optical microscope.

cracks was performed following the procedure of Fig. 1 by characterizing a crack or crack network as a function of $N/N_{failure}$ in terms of total crack length, segment length L_n, segment density and orientation α_n with respect to the specimen axis. To assure proper statistics, more than 20 000 crack segments have been analyzed. After fatigue testing the fatigue specimens were further investigated by metallographic methods and by scanning and transmission electron microscopy.

3. Results and discussion

3.1. Fatigue properties

In Fig. 2, the total stress amplitude $\Delta\sigma_t$ (a) and the total plastic strain range $\Delta\varepsilon_{pl}$ (b) are plotted as a function of the number of cycles N both for two unirradiated and two helium implanted samples. Obviously at a relatively high total strain range of $\Delta\varepsilon_t = 0.9\%$ pronounced irradiation hardening occurs during the first cycles of fatigue testing. Although this hardening undergoes substantial cyclic softening with continuing cycling and even falls below $\Delta\sigma_t$ of the unirradiated control specimen, it is sufficiently high to account for a substantial fatigue life reduction by a factor of 5. On the other hand, at relatively low total strain ranges around $\Delta\varepsilon_t = 0.5\%$, the same postirradiation treatment leads to a slightly higher fatigue life, although noticeable irradiation hardening is still visible. Another interesting feature is that at lower total strain ranges this helium implantation induced irradiation hardening does not diminish during fatigue testing. The plastic strain amplitude $\Delta\varepsilon_{pl}$ reflects the amount of inelastic deformation within one cycle, and for a given strain range $\Delta\varepsilon_t$ an increase of $\Delta\sigma_t$ is synonymous with a decrease of $\Delta\varepsilon_{pl}$ and vice versa. A comparison of Fig. 2(a) and (b) shows that this feature does not only hold for unirradiated specimens, but also for irradiated ones. The postirradiation fatigue tests performed at $\Delta\varepsilon_t = 0.9\%$ on F82H-mod specimens confirm earlier results from conventional 10–12% Cr steels [4,5], that at high strain ranges ferritic/martensitic steels show typical fatigue life reductions of a factor 5–7 after high energy proton or α-particle irradiation. To understand why postirradiation fatigue testing at different strain ranges can either lead to fatigue life increase or reduction, extensive and systematic microcrack analyses have been performed and summarized in the following.

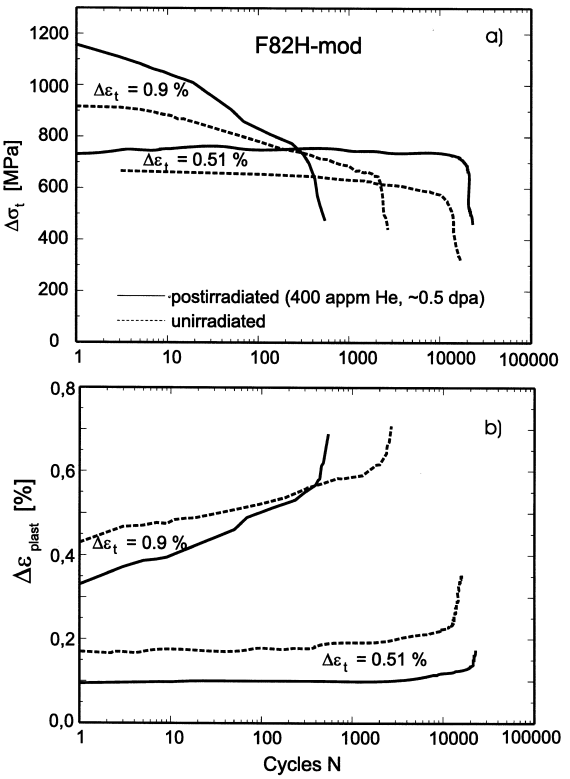

Fig. 2. Development of (a) the total stress amplitude $\Delta\sigma_t$ and (b) the total plastic strain range $\Delta\varepsilon_{pl}$ during fatigue testing of He-implanted and unirradiated specimens at high and low total strain ranges $\Delta\varepsilon_t$.

3.2. Microcrack initiation and structure

During strain controlled fatigue performed at $\Delta\varepsilon_t = 0.9\%$ all irradiated and unirradiated specimens show a high density of homogeneously distributed small microcracks, while at smaller total strain ranges of 0.4–0.51% the density of microcracks is also smaller. Apart from a few exceptions at high strain ranges, microcrack initiation and propagation are observed inside the grains, that is, the fracture behavior is completely dominated by transcrystalline cracking. Fig. 3 shows clearly that the underlying microstructure has a considerable influence on the overall crack behavior. Almost all microcracks are oriented along Cr-rich precipitates mainly of type $M_{23}C_6$. These very fine secondary precipitates were formed at inner surfaces during the final heat treatment, that is, at grain boundaries and in the vast majority of cases at lath boundaries. Obviously, microstructural barriers and the orientation of the martensite lath packets play an important role for the crack growth behavior. The microstructural analyses either revealed microcracks coming to rest usually at grain boundaries, or they showed microcrack propagation into an adjacent grain or lath packet with subsequent change of the crack orientation. A typical example for such behavior is illustrated in Fig. 3.

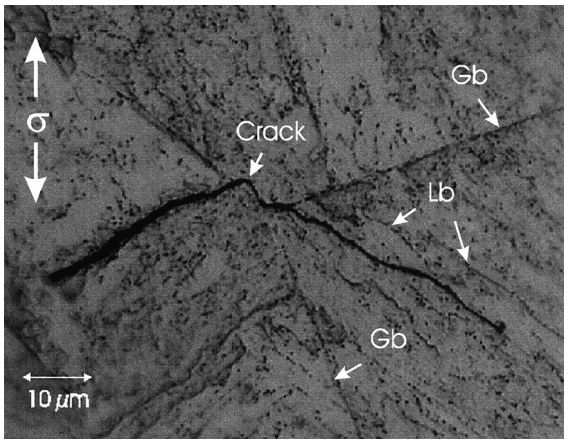

Fig. 3. Micrographs showing microcracks oriented along rows of $M_{23}C_6$ precipitates. Change of crack direction at a boundary. Grain boundaries (Gb), lath boundaries (Lb) and stress direction (σ) are indicated.

3.3. Orientation distribution of crack segments

Careful statistical investigations have shown that the orientation of the cracks is not uniformly distributed although the orientations of the martensite laths and consequently the rows of the segregated $M_{23}C_6$ precipitates are completely isotropic. With respect to the orientation distribution, the microcracks of both irradiated and unirradiated specimens can be classified into two categories: (i) low $\Delta\varepsilon_t$ and (ii) high $\Delta\varepsilon_t$. This classification is based on a determination of the angle α_n between crack segment and load axis in steps of 10° and is weighted according to the related accumulated segment length as shown in Fig. 1.

Low total strain ranges (0.4–0.51%). After intrusions and extrusions have been developed, crack initiation of carefully polished specimens starts slowly between $N/N_{\text{failure}} = 0.1$ and 0.2 with a pronounced maximum between 40° and 50°. Obviously, an angle consistent with 45° which describes the orientation of maximum shear stress in the continuum is clearly preferred in this case. Although the statistical crack analysis of the irradiated specimen showed a somewhat less pronounced angle distribution, it became obvious that at low strain ranges and perfectly polished specimen surfaces, microcrack initiation starts nearly always on intrusions and extrusions that develop in a first step in the direction of maximum shear stress along suitably oriented lath boundaries.

High total strain ranges (0.8–0.9%). After a few cycles microcrack initiation and propagation start with an orientation maximum of crack segments between 50° and 60°. This maximum can be interpreted in a natural way by a superposition of two different crack initiation processes. The first one is the already mentioned shear stress driven plastic deformation along lath boundaries oriented close to 45°, while the second component can be attributed to interface separation induced by normal stress that has its maximum at 90°. At higher strain ranges the local stress and the related plastic deformation are obviously sufficient for interface separation e.g., between primary precipitates and the matrix. Again, the angle distribution of crack segments in a helium implanted specimen is more homogeneous than in unirradiated controls.

3.4. Crack growth and coalescence

After isolated microcracks have developed during the early initiation stage to a characteristic length that depends on microstructural features, damage accumulation in unirradiated and helium implanted F82H-mod has been shown to continue in a competing manner mainly by (i) crack growth of those cracks that are able to overcome microstructural barriers as well as by (ii) coalescence of neighboring cracks. That is, at the beginning of fatigue testing one crack corresponds to a single segment, while in the damage accumulation phase either crack initiation increases the number of single cracks or the cracks propagate by keeping a low segment production rate. Depending on the total stain range and on microstructural modifications prior to fatigue testing e.g., by irradiation, either mechanism can dominate. If single cracks start to coalesce or if the segment density is very high, crack interaction can no longer be neglected. This is why in this study the analysis has been concentrated on crack segments and individual cracks rather than on the investigation of crack networks. At low strain amplitudes a low segment density is kept over more than 70% of the fatigue life, while at high strain ranges already in the early stage of fatigue testing a high density of crack segments is formed followed by network formation.

Fig. 4 shows the effect of total strain range and preimplantation of 400 appm helium on the crack growth behavior. The present investigations of the ferritic/martensitic steel F82H-mod confirm clearly the general consensus of data published on other steels [6], that during the initial phase of fatigue testing small microcracks are formed with high crack growth rates in unirradiated specimens independent of the strain range. Once the segment length has reached 75($\pm$10) μm, which corresponds closely to the mean grain diameter of this material, the crack stops or changes direction. That is, within the whole strain range the microcrack morphology in the unirradiated condition is largely controlled by microstructural barriers.

The behavior of irradiated specimens is quite different as Fig. 4 shows. At high strain ranges microstructural barriers are already surmounted during the first

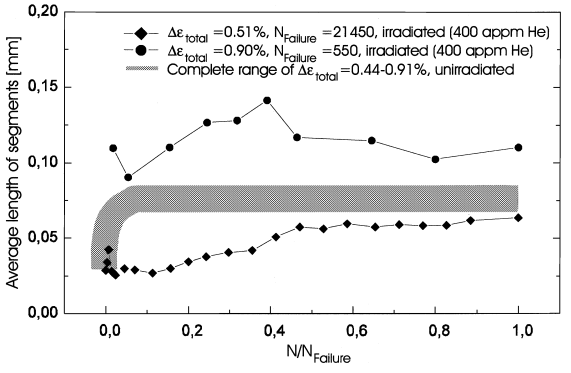

Fig. 4. Effect of strain range and preimplantation of 400 appm helium at 250°C on the fatigue crack growth behavior of the ferritic/martensitic steel F82H-mod.

few cycles. This is followed by early network formation of cracks, which leads to a reduction in fatigue life by a factor of 5. In this case, the early formation of cracks can be attributed to an increase in the total stress amplitude of almost 200 MPa [4,5,7] due to irradiation hardening that accompanied the helium implantation. On the other hand, at small $\Delta\varepsilon_{\text{total}}$ the total stress amplitude of irradiated and unirradiated specimens is not very different. In this case, the growth of microcracks is significantly impeded by very small irradiation induced defects (e.g., dislocation loops, helium bubbles, defect clusters) before they are able to reach barriers like grain and lath boundaries. That is, in spite of the observed irradiation hardening, the total stress is below a certain strain range $\Delta\varepsilon_t$ to allow very small microcracks to overcome irradiation induced obstacles.

In order to assess whether helium or displacement damage governs the irradiation induced changes of the lifetime, it should be recalled that at low strain rates the helium quantity alone has a small strengthening contribution, if any, as shown by tensile experiments performed on ferritic/martenitic steels after helium implantation [8] and neutron irradiation [9–12]. On the other hand, under dynamic loading conditions helium can contribute sensitively to embrittlement in F82H, a behavior that can be explained within a phenomenological model by fracture stress reduction due to helium segregation at inner surfaces [8]. Although advanced analytical models which take into account detailed micromechanical and microstructural features are still pending, the present fatigue experiments performed at low strain rates (Table 1) indicate that the effect of irradiation on lifetime is governed at lower irradiation temperatures by stress induced propagation of microcracks. Depending on the amount of irradiation induced hardening, this can lead either to fatigue life reduction at high $\Delta\varepsilon_t$ or to fatigue life increase at low $\Delta\varepsilon_t$. A detailed model describing microcrack interaction and coalescence by elasto-plastic fracture mechanics analysis and a neural network is given in [13].

4. Summary and conclusions

In fatigue tests, unirradiated specimens follow a typical lifetime distribution in accordance with the Coffin–Manson law. All irradiated specimens show irradiation induced hardening and a correlated loss of plasticity. At higher strain ranges ($\Delta\varepsilon_{\text{total}} = 0.9\%$), the lifetime of the irradiated specimen is distinctly reduced, while at lower strain ranges ($\Delta\varepsilon_{\text{total}} \leqslant 0.5\%$), irradiated specimens show a slightly increased lifetime. The very small cracks have been classified by their length, orientation, density and coalescence behavior. Subsequent metallographic and microstructural investigations revealed crack initiation mainly along martensitic laths and transgranular crack propagation, partly affected by the orientation of martensitic bands in adjacent grains. Based on more than 20 000 crack segments, a statistical analysis of the crack formation and propagation processes was performed.

Characteristic differences between unirradiated and irradiated specimens were observed in terms of length and orientation distribution of crack segments, indicating different types of microstructural barriers for crack propagation. In the unirradiated condition during the initial phase of fatigue testing small microcracks are formed with high crack growth rates independent of the stain range. Once the segment length has reached $75(\pm 10)$ μm, which corresponds closely to the mean grain diameter, the crack stops or changes direction. While in the unirradiated condition the microcrack morphology is controlled largely by microstructural barriers, the behavior of irradiated specimens can be quite different. Depending on strain range and irradiation condition, microcrack initiation might be either accelerated, resulting in fatigue life reduction by a factor 5, or it can be impeded by very small irradiation induced defects. In order to achieve the highest possible lifetime in irradiated and fatigue loaded ferritic/martensitic steels, it is therefore necessary (i) to reduce the grain size as much as possible by a proper selection of the heat treatment, and (ii) to keep the total strain in related blanket designs below a limit of about 0.5%.

Acknowledgements

The authors would like to express their appreciation to Professor K. Ehrlich for many helpful discussions. This work has been performed in the framework of the Nuclear Fusion Project of Forschungszentrum Karlsruhe and is supported by the European Union within the European Fusion Technology Program.

References

[1] A. Hishinuma, A. Kohyama, R.L. Klueh, D.S. Gelles, W. Dietz, K. Ehrlich, J. Nucl. Mater. 258–263 (1998) 193.
[2] K. Ehrlich, D.R. Harries, A. Möslang, Characterization and assessment of ferritic/martensitic steels, Report FZKA 5626, February 1997.
[3] A. Möslang, S. Baumgärtner, G. Bürkle, R. Lindau, G. Przykutta, K. Ehrlich, in: C. Ferro, M. Casparotto, H. Knoepfel (Eds.), Proceedings of the 17th Symposium on Fusion Technology, Rome, September 1992, North-Holland, Amsterdam, 1993, p. 1439.
[4] P. Marmy, J. Nucl. Mater. 212–215 (1994) 594.
[5] R. Lindau, A. Möslang, J. Nucl. Mater. 212–215 (1994) 599.
[6] L.A. James, At. Energy Rev. 14 (1976) 37.
[7] J. Bertsch, R. Lindau, A. Möslang, J. Nucl. Mater. 233–237 (1996) 276.
[8] R. Lindau, A. Möslang, D. Preininger, M. Rieth, H.D. Röhrig, J. Nucl. Mater. 272 (1999) 450.
[9] R.L. Klueh, G.J. Alexander, J. Nucl. Mater. 218 (1995) 151.
[10] D.S. Gelles, J. Nucl. Mater. 230 (1996) 187.
[11] R.L. Klueh, G.J. Alexander, J. Nucl. Mater. 230 (1996) 191.
[12] K. Shiba, M. Suzuki, A. Hishinuma, J. Nucl. Mater. 233–237 (1996) 309.
[13] S. Meyer, E. Diegele, A. Brückner-Foit, A. Möslang, Fatigue Fract. Eng. Mater. Struct. (2000) in press.